Available online at www.sciencedirect.com
ScienceDirect
Scripta Materialia 60 (2009) 532–535
Scripta MATERIALIA
www.elsevier.com/locate/scriptamat

Are nanotwinned structures in fcc metals optimal for strength, ductility and grain stability?

Yashashree Kulkarni,[a,*] Robert J. Asaro[a] and Diana Farkas[b]

[a] *Department of Structural Engineering, University of California, San Diego, 9500 Gilman Drive, Mail Code 0085, La Jolla, CA 92093, USA*

[b] *Department of Materials Science and Engineering, Virginia Tech, Blacksburg, VA 24061, USA*

Received 11 September 2008; revised 27 November 2008; accepted 1 December 2008
Available online 13 December 2008

The optimality of nanotwinned structures in imparting maximum strength and stability has been investigated by performing atomistic simulations of dislocation interactions with various types of grain boundaries. By developing an understanding of the mechanism of the instability, we predict that nanocrystalline metals with grain sizes below 50 ± 10 nm or 70 ± 10 nm (in Cu) are inherently unstable at 0 or 300 K, respectively, in contrast to nanotwinned face-centered cubic structures which are stable and optimal.

Keywords: Nanotwins; Grain stability; Nanocrystalline metals; Nanoindentation

It is well established that the large excess energy associated with grain boundaries in nanocrystalline (nc) metals leads to instability in the grain structure: in particular, under conditions of suitably high stress, grains grow and the high-strength characteristic of nc metals decreases [1–5]. Interestingly, grain growth in nc Cu was found to occur faster (and with accumulated strain) at cryogenic temperatures [2], which suggests that the instability of ultrafine grains is driven by high stresses, rather than solely by accumulation of plastic strains. The fact that the flow stress is much higher at lower temperatures, coupled to the high sensitivity to strain rate [6], is consistent with these observations and suggestions of a stress-based instability. A mechanistic explanation is, however, lacking to date but these observations raise several fundamental questions that may be answered by a mechanistic understanding: (i) what are the critical conditions that trigger grain boundary motion leading to grain growth; (ii) is there a limiting grain size (and thereby strength level) below (or above) which the instability is inevitable; and (iii) are there grain boundary types, and thus nc structural motifs, that are optimal? We explored these questions using an atomistic approach by simulating the interaction of dislocations generated via nanoindentation in Cu samples that contain a variety of boundary types, including tilt and coherent twin boundaries. We generated intense states of stress by simulating nanoindentation of bicrystal "specimens" containing the various boundaries located at different depths beneath the indentation surface. Indentation also served to introduce dislocations into one of the grains separated by twin or tilt boundaries. We then followed the interaction of the emitted dislocations with the boundaries. Perhaps not surprisingly we find that nanotwinned structures are among the most stable in addition to providing optimal strength and ductility; twin boundaries, in fact, possess minimal excess energy yet effectively block slip dislocations. Such optimal performance has been experimentally documented in macroscopic tests on nanotwinned Cu synthesized by pulsed electrodeposition [7] and explained mechanistically via continuum dislocation modeling [8]. The issue of grain (and grain boundary) stability has remained unaddressed, and for this an atomistic approach seemed necessary.

We began by studying the response of typical boundary types to a uniformly imposed shear deformation. Specifically, we considered a $\Sigma 3(1\,1\,1)$ coherent twin boundary (CTB) and a $\Sigma 9(2\,2\,1)$ symmetrical tilt boundary. The contours of shear stresses show that the tilt boundary has very high local periodic stresses due to the misfit in crystal orientations above and below the tilt

* Corresponding author. Tel.: +1 626 372 1474; e-mail: ykulkarni@ucsd.edu

1359-6462/$ - see front matter © 2008 Acta Materialia Inc. Published by Elsevier Ltd. All rights reserved.
doi:10.1016/j.scriptamat.2008.12.007

boundary, whereas the CTB does not lead to any stresses in the relaxed state. We also note the recent molecular dynamic (MD) simulations of Cahn et al. [9] who studied the coupled shear/normal motion of a range of tilt boundaries. Effectively they found that when symmetric tilt boundaries are subject to uniform shear parallel to the plane of the boundary, they undergo a motion in the direction normal to the boundary's plane. Such motion would lead to grain growth, thus inducing instability in ultrafine structure. Related studies have been performed by Sansoz and Molinari [10,11]. They likewise observed coupled shear/normal boundary motion, but also noted profuse defect generation accompanying boundary shear at many of their tilt boundaries.

In our shear simulations, we used face-centered cubic (fcc) bicrystals of copper, 6 nm × 8 nm × 8 nm in size, with the grain boundary located at the center and normal to the z-direction ((1 1 1) in case of the CTB and (2 2 1) in case of the tilt boundary). Boundary conditions involved imposing a uniform shearing translation of the upper surfaces while keeping the bottom surface fixed. Periodic boundary conditions were applied in the lateral directions. The displacement was prescribed in increments of 0.2 Å along $[\bar{1}\,1\,2]$ in case of the bicrystal with a CTB and along $[1\,1\,\bar{4}]$ in case of the bicrystal with a tilt boundary. Quasi-static simulations were performed using the finite-temperature quasicontinuum code (FTQC) developed recently by Kulkarni et al. [12]. Since these simulations were performed at 0 K with full atomistic resolution, the equilibrium configurations were determined by minimizing the potential energy of the system expressed through the use of the embedded-atom (EAM) interatomic potential proposed by Johnson [13]. The resulting shear stress vs. shear strain is shown in Figure 1. The inserts show "snapshots" of the atomistic configurations in the vicinity of the grain boundary and the top surface extracted using the centrosymmetry parameter [14]. MD simulations were also carried out at 300 K and at various strain rates. The results are discussed below but not included herein due to limitations of space.

The responses of the two types of boundary differ in several distinct and important ways. For one, the shear stress vs. shear displacement response of the CTB displays a rather perfect "saw-tooth" pattern which corresponds, with each peak, to the uniform motion of the boundary; the direction of motion is normal to the plane of the boundary, as described by Cahn et al. [9]. The shear stress required to induce such motion is just over 3 GPa, testifying to the high shear strength of CTBs.

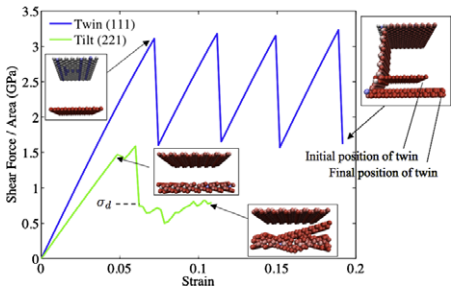

Figure 1. Shear stress vs. shear strain plots for the uniform shear of a symmetrical tilt boundary (green) and a CTB (blue) at 0 K.

Moreover, the boundary retains its atomistic configuration (and perfection) and thereby its high strength during the process of repeated shearing. In contrast, the tilt boundary "yields" at a much lower strength (~1.5 GPa) and does so with the production of defects that propagate into the surrounding grain matrices. Consequently, the sustainable shear strength of the tilt boundary decreases. This is consistent with the findings of Sansoz and Molinari [11] that just after initial shear, the shear strength of the boundary fell to values of the order of one-half the initial strength; this is indicated in Figure 1 as σ_d, using the notation found in Ref. [11].

We next simulated the process of nanoindentation of a bicrystal cell; the force vs. indentation curves for the $\Sigma3(1\,1\,1)$ CTB and the $\Sigma9(2\,2\,1)$ tilt boundary are shown in Figure 2a and b, respectively. The simulation cells used were 10 nm × 10 nm × 10 nm in size, the crystallographic orientations being the same as before. The spherical indenter was modeled using an external potential given by:

$$\Phi^{\text{ext}}(r) = AH(R-r)(R-r)^3,$$

where A is a force constant taken to be 5 eV Å^{-3} in the present calculations and $H(r)$ is the step function [14]. $R = 50$ Å is the radius of the indenter and r denotes the position vector of an atom. The indentation was performed quasi-statically using an incremental vertical displacement of 0.2–0.01 Å. As before, periodic boundary conditions were applied in the lateral directions, and the simulations were carried out at 0 K.

The example of a CTB located 1.2 nm below the indentation surface is most revealing. Elastic response during indentation is characterized by a roughly parabolic load vs. indentation curve as seen at the lower loads in Figure 2a; at the load indicated by the leftmost arrow, departure from elastic response is observed. The locally maximum shear stress acting on the twin bound-

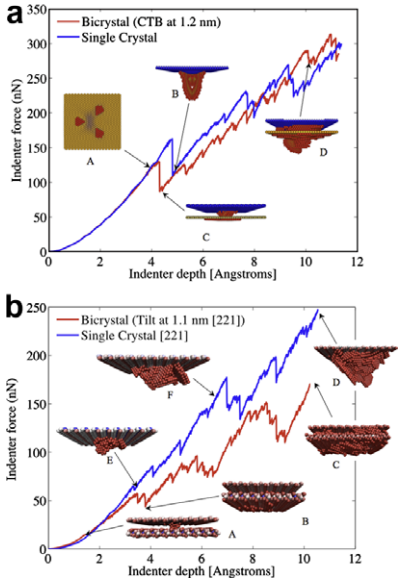

Figure 2. Force vs. indentation depth curves resulting from nanoindentation at 0 K on (a) $[1\,\bar{1}\,1]$ surface of a bicrystal with a CTB and a single crystal of Cu and (b) [2 2 1] surface of a bicrystal with a $\Sigma9(2\,2\,1)$ symmetrical tilt boundary and a single crystal of Cu.

ary here was, in fact, ~3 GPa. The atomistic configuration in inset A in Figure 2a shows the nucleation of boundary dislocations inducing shear of the CTB. No dislocations had yet been emitted at the indentation surface. Thus, under highly nonuniform states of stress, CTBs respond in much the same manner as just described for ideal CTBs subject to uniform shear. This process of localized twin boundary shear is coupled to a normal motion of the boundary segment undergoing shear. At somewhat higher indenter loads, partial dislocations are generated at the indentation surface, which immediately (i.e. with no measurable additional indentation) propagate and impinge on the boundary, leading to a sudden load drop. The inset C in Figure 2a shows that the impinging partial dislocation is absorbed within the boundary as described in the continuum dislocation model of Asaro and Kulkarni [8]. The absorbed partial dislocation causes the CTB to shear and induces a coupled normal motion of those areas of the CTB undergoing shear. Dislocation transmission through the CTB is seen to be difficult and is only observed at much higher loads (and local shear stresses) as illustrated by inset D. Yet another observation of note is that despite considerable defect generation and plastic deformation, the bicrystal retains its "hardness"; in fact, the load vs. indentation curve rises even above that of the single crystal.

The effectiveness of twin boundaries in blocking fcc Shockley partial dislocations has also been observed in the MD simulations of Cao and Wei [17] and has been studied in detail by Jin et al. [18]. This was also confirmed in our MD simulations of tensile deformation of nc Cu containing twins. The twinned sample was created by Voronoi construction of random grains with an initial diameter of 5 nm. The sample was then annealed, as described in Ref. [19], resulting in a final grain size of 8 nm and a large number of annealing twins. MD simulations were performed using the LAMMPS code [15] by subjecting the annealed sample to a tensile deformation at 300 K and a strain rate of $3.33 \times 10^8\ s^{-1}$. Figure 3 shows a slice of the initial structure and the corresponding slice after 5% tensile deformation. The random grain boundaries and CTBs are visible through coloring that corresponds to the centrosymmetry parameter [14]. The circled region in Figure 3b shows examples of where dislocations were emitted from random boundaries and blocked by annealing twins. Atomistic detail of the interaction of an impinging dislocation with a twin boundary is shown in Figure 3c. In agreement with our observations above, the dislocation is absorbed on the CTB as evidenced by the "step" that was created.

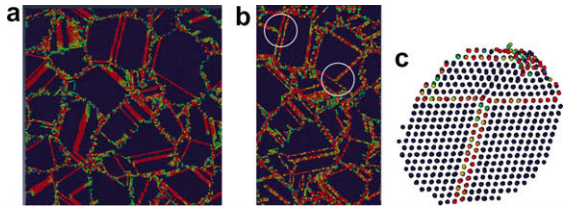

Figure 3. Effect of annealing twins in nanocrystalline Cu. (a) Initial structure containing annealing twins. (b) Deformed structure in which circled regions show examples of dislocation emission at random boundaries and where they were blocked at CTBs. (c) Atomistic detail of the interaction of an impinging dislocation with a CTB.

In contrast to the behavior of a CTB, Figure 2b shows results for indentation of a bicrystal containing the $\Sigma 9(221)$ tilt boundary. Dislocations generated at the indentation surface impinge on the boundary as seen in inset A but, unlike the case of the CTB, are more readily transmitted as seen by the defect generation evident in inset B. Absorption onto the tilt boundary is not observed, unlike the CTB, which is itself a slip plane for an fcc crystal. One overall result is that the bicrystal's "hardness" degrades as evidenced by the load vs. indentation curve falling considerably below that of the single crystal. The tilt boundary loses its hardening effect and instead becomes a source of dislocations that then contribute to plastic deformation. For our $\Sigma 9(221)$ tilt boundary, this reduced strength is of order $\sigma_d \sim 0.5$–0.7 GPa. Sansoz and Molinari [11] report the reduced strength to be in the range $\sigma_d \sim 0.62$–0.87 GPa for about one-half of their tilt boundaries.

Taken together, these results confirm that CTBs are initially very effective barriers to dislocation motion and remain so even during defect generation accompanying plastic deformation. In contrast, tilt boundaries, i.e. with $\Sigma \geqslant 5$, "yield" at much lower stresses and, when impinged on by slip dislocations, offer much lower resistance to dislocation transmission into the adjoining grain and can act as sources of defects that contribute to ongoing plastic deformation. These results are further supported by the MD simulations of Jang and Farkas [20] who studied dislocation interactions with a semicoherent $\Sigma 5(210)$ tilt boundary. They observed modest increases in the resistance to indentation for a bicrystal containing the tilt boundary. One interpretation of these results is an alternation between the role of grain/twin boundaries as barriers for dislocation motion and/or as preferred sites for dislocation emission. For special boundaries such as coherent twins, i.e. with low Σ, the role of barriers dominates, whereas for higher Σ and random boundaries, their role as dislocation sources can dominate, especially if there are no other sources present.

In order to understand the effect of temperature and strain rate on the deformation mechanisms discussed above, we also performed molecular dynamics simulations of boundary shear in LAMMPS using the EAM potential of Daw and Baskes [16]. The simulations were carried out at 0 and 300 K and at shearing rates of 3×10^6, 3×10^7 and $3 \times 10^8\ s^{-1}$. The results were fitted to the simple rate form:

$$\dot{\gamma} = \dot{\gamma}_0 e^{-\{Q - \tau v\}/kT}$$

for the purpose of extracting estimates for the activation volume, v, and thus, the rate sensitivity. "τ" denotes the shear stress on the boundary plane along the shearing direction. Results for both types of boundary were consistent with the FTQC simulations, although the Daw and Baskes potential [16] in LAMMPS yielded peak shear stresses 5–10% below those obtained using the Johnson potential [13] in the FTQC simulations. For the $\Sigma 3(111)$ CTB, it was found that $v \approx 3.18 \times 10^{-28}\ m^3 \approx 18b^3$ with b being the perfect

Burger's vector in fcc Cu. Using this in the rate law above, the peak shear stress at 300 K, extrapolated to a typical experimental strain rate of $10^{-3}\,s^{-1}$, is estimated to be 2.1 GPa. For the $\Sigma 9(2\,2\,1)$ tilt boundary, on the other hand, a similar simulation showed that v was much smaller ($\sim 4b^3$) and thus the peak shear stress at 300 K and strain rate of $10^{-3}\,s^{-1}$ falls well below 1 GPa.

Nanocrystalline fcc metals, and in particular nc Cu, with grain sizes approaching 10 nm have been reported to have yield strengths of the order of ~1 GPa [4]. Zhu et al. [5], however, have considered in their analysis the actual distribution of grain sizes that exists in most all nc metals tested to date. The fact is that most of the strain (over 80% in a simulated uniaxial tensile test) is carried by grains whose sizes are considerably larger than that of the average grain. Thus the smaller (and potentially unstable) grains are more highly stressed. Zhu et al.'s model analysis [5] of nc Cu would estimate, for example, the local stresses in small grains with diameters in the range 10–15 nm to be of the order of 2 GPa in an aggregate with a mean grain size of 20 nm. We thereby anticipate that the smaller grains are potentially unstable. Those potentially unstable grains would be capable of bearing a stress (again using uniaxial tension as the deformation mode and with the drop in shear stress extracted from Fig. 2) on the order of $2 \times (0.5\text{–}0.87)$ GPa and remain stable, using the full range of boundary strengths cited above. Thus tensile strengths on the order of 1–1.8 GPa suggest potentially unstable grain structures, at least for boundaries such as tilt boundaries. Using the data shown in Figure 1b of Dao et al. [4], which plots yield strength vs. grain diameter, this would estimate the critical grain size to be of order $\sim 50 \pm 10$ nm. At 300 K, and with imposed quasi-static strain rates, this critical grain size would be larger, of the order of $\sim 70 \pm 10$ nm, since the peak strength is no larger than 1 GPa. CTBs, on the other hand, possess much higher sustainable strengths (~3 GPa at 0 K and ~2.1 GPa at 300 K), and thus recalling the data of Lu et al. [7], we would suggest that even their finest twin lamella spacing (~20 nm) would be stable, at 0 K or even at 300 K. The suggestion of this analysis is, therefore, that nc fcc metals whose ultrafine structure relies on tilt, or high-angle random boundaries will be prone to grain size instability at grain sizes below, say, 50 ± 10 nm at 0 K, or $\sim 70 \pm 10$ nm at 300 K. We note that these critical size estimates are completely consistent with similar estimates based on experimental data obtained via high-pressure torsion [3]. We envision the process being driven by high stresses sufficient to cause boundary motion. It is important to note, however, that the accumulation of inelastic strains is an inherent part of the process of boundary motion, and thus in deformation scenarios involving only relatively small strains, grain growth may not be observed. Thus during either microindentation [2] or high-pressure torsion [3], grain growth is expected, whereas during uniaxial tension where inelastic strains are typically below 10%, grain growth may not be observed. On the other hand, nanotwinned structures appear to be quite stable at even very high stresses and thus may represent an optimal motif.

The original report of Lu et al. [7] and the review of Dao et al. [4] noted additional advantages of nanotwinned structures vs. nanocrystalline structures namely, inter alia, far less loss in conductivity, and quite importantly, high ductility. Taken together with the analysis here of grain stability, this may well provide more than enough impetus for developing processing routes for the synthesis of bulk nanotwinned fcc metals as an alternative to nc structures with tilt and high-angle boundaries. Of course, the true optimization of nanotwinned structures will also require additional attention to be paid to possible adverse phenomena such as boundary-affected diffusion and resulting microvoid formation as recently documented by Chen et al. [21].

This work was partially supported by the National Science Foundation through an allocation of advanced computing resources provided by San Diego Supercomputer Center.

[1] M. Jin, A.M. Minor, E.A. Stach, J.W. Morris Jr., Acta Mater. 52 (2004) 5381.
[2] K. Zhang, J.R. Weertman, J.A. Eastman, Appl. Phys. Lett. 87 (2006) 061921.
[3] X.Z. Liao, A.R. Kilmametov, R.Z. Valiev, H. Gao, X. Li, A.K. Mukherjee, J.F. Bingert, Y.T. Zhu, Appl. Phys. Lett. 88 (2006) 021909.
[4] M. Dao, L. Lu, R.J. Asaro, J. De Hosson, E. Ma, Acta Mater. 55 (2007) 4041.
[5] B. Zhu, R.J. Asaro, P. Krysl, K. Zhang, J. Weertman, Acta Mater. 54 (2006) 3307.
[6] R.J. Asaro, S. Suresh, Acta Mater. 53 (2005) 3369.
[7] L. Lu, Y. F Shen, X.H. Chen, L.H. Qian, K. Lu, Science 304 (2004) 422.
[8] R.J. Asaro, Y. Kulkarni, Scripta Mater. 58 (2008) 389.
[9] J.W. Cahn, Y. Mishin, A. Suzuki, Acta Mater. 54 (2006) 4953.
[10] F. Sansoz, J.F. Molinari, Scripta Mater. 50 (2004) 1283.
[11] F. Sansoz, J.F. Molinari, Acta Mater. 53 (2005) 1931.
[12] Y. Kulkarni, J. Knap, M. Ortiz, J. Mech. Phys. Solids 56 (2008) 1417.
[13] R.A. Johnson, Phys. Rev. B 37 (1988) 3924.
[14] C.L. Kelchner, S.J. Plimpton, J.C. Hamilton, Phys. Rev. B 58 (1998) 11085.
[15] S.J. Plimpton, J. Comput. Phys. 117 (1995) 1.
[16] M.S. Daw, M.I. Baskes, Phys. Rev. B 29 (1984) 6443.
[17] A. Cao, Y. Wei, J. Appl. Phys. 102 (2007) 083511.
[18] Z.-H. Jin, P. Gumbsch, K. Albe, E. Ma, K. Lu, H. Gleiter, H. Hahn, Acta Mater. 56 (2008) 1126.
[19] D. Farkas, E. Bringa, A. Caro, Phys. Rev. B 75 (2007) 184111.
[20] H. Jang, D. Farkas, Mater. Lett. 61 (2007) 868.
[21] K.-C. Chen, W.-W. Wu, C.-N. Liao, L.-J. Chen, K.N. Tu, Science 321 (2008) 1066.